A Cartesian Parametrization for the Analysis of Material Instability

Alejandro Mota[1], Qiushi Chen[2]*,
James W. Foulk III[1], Jakob T. Ostien[1], Zhengshou Lai[2]

[1]Mechanics of Materials Department
Sandia National Laboratories
Livermore CA 94550, USA

[2]Glenn Department of Civil Engineering
Clemson University
Clemson, SC 29631, USA

July 3, 2015

Abstract

We propose a Cartesian parametrization for vectors to test for the loss of the ellipticity condition in the analysis of material instability.

The parametrization is used to construct a tensor that is the acoustic tensor multiplied by a scalar factor. It is shown that both tensors become singular at the same time and in the same planes in the presence of a material instability.

The performance of the Cartesian parametrization is compared against other common and uncommon parametrizations of the acoustic tensor. The results of these comparisons show that the Cartesian parametrization is more robust and more numerically efficient than the other tested parametrizations in general.

1 Introduction

The analysis of material instability plays an important role in the simulation of constitutive behavior. A reliable method for the detection of material instability is required whether one

*Email: qiushi@clemson.edu

is interested in studying the instability itself or to devise numerical regularization methods that prevent lack of convergence once an instability is present.

Herein we adopt the definition of material instability as the loss of the *strong ellipticity condition*, which is equivalent to the loss of the *strong Legendre-Hadamard condition* for stored energy densities that are twice continuously differentiable [1].

1.1 Previous Work

Extensive work has been done on the subject of material instabilities. See Armero and Garikipati [2] and Miehe, Lambrecht, and Gürses [14] for a brief historical overview of the development of classical localization analysis, starting with the seminal work of Hadamard [8], followed by Thomas [20], Hill [9], Rice [18] and others.

In all these works, the criterion for determining the existence of a material instability is the loss of the strong ellipticity condition.

Assumptions [3].

2 General Framework

The determination of the loss of the strong ellipticity condition for a very general class of materials can be achieved by recourse to incremental variational constitutive updates. Within this framework, an incremental stress potential embodies the constitutive behavior of the material during a time increment, including elasticity, viscoelasticity, viscoplasticity, and rate dependence [4, 6, 12, 14–16, 22].

2.1 Variational Constitutive Updates

The mechanical response of the solids considered here is characterized by a dissipation potential of the form

$$D(\boldsymbol{F}, \dot{\boldsymbol{F}}, \boldsymbol{Z}, \dot{\boldsymbol{Z}}) = \dot{A}(\boldsymbol{F}, \boldsymbol{Z}) + \phi(\boldsymbol{F}, \dot{\boldsymbol{F}}, \boldsymbol{Z}) + \psi^*(\boldsymbol{Z}, \dot{\boldsymbol{Z}}), \tag{2.1}$$

in which $A(\boldsymbol{F}, \boldsymbol{Z})$ is the Helmholtz free-energy density, $\phi(\boldsymbol{F}, \dot{\boldsymbol{F}}, \boldsymbol{Z})$ is a viscous potential, $\psi^*(\boldsymbol{Z}, \dot{\boldsymbol{Z}})$ is a dual kinetic potential or dissipation function, $\boldsymbol{F}$ is the deformation gradient and $\boldsymbol{Z}$ is a collection of suitable internal variables that describe the state of the material at a given point. The first Piola-Kirchhoff stress and the conjugate thermodynamic forces to $\boldsymbol{Z}$ are given by

$$\boldsymbol{P} = \frac{\partial D}{\partial \dot{\boldsymbol{F}}}(\boldsymbol{F}, \dot{\boldsymbol{F}}, \boldsymbol{Z}, \dot{\boldsymbol{Z}}) = \frac{\partial A}{\partial \boldsymbol{F}}(\boldsymbol{F}, \boldsymbol{Z}) + \frac{\partial \phi}{\partial \dot{\boldsymbol{F}}}(\boldsymbol{F}, \dot{\boldsymbol{F}}, \boldsymbol{Z}), \quad \boldsymbol{Y} = -\frac{\partial A}{\partial \boldsymbol{Z}}(\boldsymbol{F}, \boldsymbol{Z}), \tag{2.2}$$

respectively. In order to ensure a variational structure, we have postulated the existence of a dual kinetic potential or dissipation function $\psi^*(\boldsymbol{Z}, \dot{\boldsymbol{Z}})$ such that

$$\boldsymbol{Y} = \frac{\partial \psi^*}{\partial \dot{\boldsymbol{Z}}}(\boldsymbol{Z}, \dot{\boldsymbol{Z}}). \tag{2.3}$$

Next, we minimize the dissipation potential (2.1) with respect to the internal variable rates as

$$\begin{aligned}\inf_{\dot{\boldsymbol{Z}}}[D(\boldsymbol{F},\dot{\boldsymbol{F}},\boldsymbol{Z},\dot{\boldsymbol{Z}})] &= \inf_{\dot{\boldsymbol{Z}}}\left[\dot{A}(\boldsymbol{F},\boldsymbol{Z})+\psi^*(\boldsymbol{Z},\dot{\boldsymbol{Z}})\right]+\phi(\boldsymbol{F},\dot{\boldsymbol{F}},\boldsymbol{Z}),\\ &= \inf_{\dot{\boldsymbol{Z}}}\left[\frac{\partial A}{\partial \boldsymbol{F}}(\boldsymbol{F},\boldsymbol{Z}):\dot{\boldsymbol{F}}+\frac{\partial A}{\partial \boldsymbol{Z}}(\boldsymbol{F},\boldsymbol{Z})\cdot\dot{\boldsymbol{Z}}+\psi^*(\boldsymbol{Z},\dot{\boldsymbol{Z}})\right]+\phi(\boldsymbol{F},\dot{\boldsymbol{F}},\boldsymbol{Z}),\end{aligned} \tag{2.4}$$

which in turn leads to Biot's equation for standard dissipative systems

$$\frac{\partial A}{\partial \boldsymbol{Z}}(\boldsymbol{F},\boldsymbol{Z})+\frac{\partial \psi^*}{\partial \dot{\boldsymbol{Z}}}(\boldsymbol{Z},\dot{\boldsymbol{Z}})=\boldsymbol{0}. \tag{2.5}$$

Approximate solutions to this equation may be found by recourse to the incremental energy density function for a time increment $t\in[t_n,t_{n+1}]$

$$w(\boldsymbol{F}_{n+1},\boldsymbol{Z}_{n+1}):=\int_{t_n}^{t_{n+1}}\left[\dot{A}(\boldsymbol{F},\boldsymbol{Z})+\phi(\boldsymbol{F},\dot{\boldsymbol{F}},\boldsymbol{Z})+\psi^*(\boldsymbol{Z},\dot{\boldsymbol{Z}})\right]\,dt, \tag{2.6}$$

in which the integral is evaluated using a midpoint-like rule as follows

$$\begin{aligned}w(\boldsymbol{F}_{n+1},\boldsymbol{Z}_{n+1})\approx& A(\boldsymbol{F}_{n+1},\boldsymbol{Z}_{n+1})-A(\boldsymbol{F}_n,\boldsymbol{Z}_n)+\\ &\triangle t\left[\phi\left(\boldsymbol{F}_{n+\alpha},\frac{\triangle\boldsymbol{F}}{\triangle t},\boldsymbol{Z}_{n+\alpha}\right)+\psi^*\left(\boldsymbol{Z}_{n+\alpha},\frac{\triangle\boldsymbol{Z}}{\triangle t}\right)\right].\end{aligned} \tag{2.7}$$

with

$$\triangle t:=t_{n+1}-t_n,\quad \triangle\boldsymbol{F}:=\boldsymbol{F}_{n+1}\boldsymbol{F}_n^{-1},\quad \triangle\boldsymbol{Z}:=\boldsymbol{Z}_{n+1}-\boldsymbol{Z}_n, \tag{2.8}$$

and

$$\begin{aligned}\boldsymbol{F}_{n+\alpha}&:=\exp[(1-\alpha)\log\boldsymbol{F}_n+\alpha\log\boldsymbol{F}_{n+1}],\\ \boldsymbol{Z}_{n+\alpha}&:=(1-\alpha)\boldsymbol{Z}_n+\alpha\boldsymbol{Z}_{n+1},\end{aligned} \tag{2.9}$$

where α is an algorithmic parameter. In order to obtain an explicit scheme, we choose $\alpha=0$. Next, we define the incremental stress potential as

$$\begin{aligned}W(\boldsymbol{F}_{n+1}):=&\inf_{\boldsymbol{Z}_{n+1}}[w(\boldsymbol{F}_{n+1},\boldsymbol{Z}_{n+1})]\\ =&\inf_{\boldsymbol{Z}_{n+1}}\left[A(\boldsymbol{F}_{n+1},\boldsymbol{Z}_{n+1})-A(\boldsymbol{F}_n,\boldsymbol{Z}_n)+\triangle t\psi^*\left(\boldsymbol{Z}_n,\frac{\triangle\boldsymbol{Z}}{\triangle t}\right)\right]+\\ &\triangle t\phi\left(\boldsymbol{F}_n,\frac{\triangle\boldsymbol{F}}{\triangle t},\boldsymbol{Z}_n\right).\end{aligned} \tag{2.10}$$

This minimization provides an optimal path for the internal variables $\boldsymbol{Z}$ in the time increment $t\in[t_n,t_{n+1}]$. Furthermore, the Euler-Lagrange equation corresponding to (2.10) is

$$\frac{\partial A}{\partial \boldsymbol{Z}_{n+1}}(\boldsymbol{F}_{n+1},\boldsymbol{Z}_{n+1})+\triangle t\frac{\partial\psi^*}{\partial\boldsymbol{Z}_{n+1}}\left(\boldsymbol{Z}_n,\frac{\triangle\boldsymbol{Z}}{\triangle t}\right)=\boldsymbol{0}. \tag{2.11}$$

which is a discrete version of Biot's equation (2.5) [13]. The incremental first Piola-Kirchhoff stress and tangent moduli can be computed in turn as

$$\boldsymbol{P}_{n+1} := \frac{\partial W}{\partial \boldsymbol{F}}(\boldsymbol{F}_{n+1}), \quad \mathbb{C}_{n+1} := \frac{\partial^2 W}{\partial \boldsymbol{F}^2}(\boldsymbol{F}_{n+1}), \tag{2.12}$$

respectively. Thus, by using variational constitutive updates, the stress and the tangent moduli can be derived from the hyperleastic-like potential (2.10) for a very general class of constitutive behavior that may include viscosity and rate dependence. This in turn provides the means to apply the classical analysis tools that are used in hyperelasticity for complex materials as well.

2.2 The Strong Ellipticity Condition

For simplicity in notation and unless otherwise stated, henceforth we omit the time indices n and $n+1$ with the understating that further developments take place at time t_{n+1}.

The ellipticity condition can be expressed as

$$(\boldsymbol{m} \otimes \boldsymbol{n}) : \mathbb{C} : (\boldsymbol{m} \otimes \boldsymbol{n}) \geq 0, \quad \forall\, \boldsymbol{m}, \boldsymbol{n} \in \mathbb{R}^3. \tag{2.13}$$

If the condition holds strictly for non-zero vectors $\boldsymbol{m}$ and $\boldsymbol{n}$, then it is called the strong ellipticity condition [8, 14, 21]. It is customary to *assume* that $\boldsymbol{m}$ and $\boldsymbol{n}$ are unit vectors, *i.e.* $\boldsymbol{m}, \boldsymbol{n} \in S^2$ where $S^2 := \{\boldsymbol{t} \in \mathbb{R}^3 \,|\, \|\boldsymbol{t}\| = 1\}$ is the unit sphere. Define the acoustic tensor as

$$\boldsymbol{A} := \boldsymbol{n} \cdot \mathbb{C} \cdot \boldsymbol{n} \quad \text{or} \quad A_{jk} := n_i C_{ijkl} n_l, \quad \boldsymbol{n} \in S^2, \tag{2.14}$$

then the strong ellipticity condition becomes

$$\boldsymbol{m} \cdot \boldsymbol{A} \cdot \boldsymbol{m} > 0, \quad \boldsymbol{m} \in S^2. \tag{2.15}$$

In order to satisfy the strong ellipticity condition, the acoustic tensor must be positive definite. Therefore, (2.13) and (2.15) reduce to

$$\det \boldsymbol{A} > 0, \tag{2.16}$$

which provides a method to determine the onset of a material instability.

2.3 Bifurcation

By using the strong ellipticity condition (2.13) or its equivalent with the acoustic tensor (2.16), the detection of bifurcation or loss of ellipticity in the material is fully characterized by its fourth-order tangent moduli (2.12). The onset of bifurcation is then posed as a minimization problem. First we assume that the normal vector $\boldsymbol{n}$ is parametrized by a set of parameters $\boldsymbol{q}$, thus turning the determinant of the acoustic tensor $\det \boldsymbol{A}$ into a function

of $\boldsymbol{q}$. Then the determinant of the acoustic tensor $\det \boldsymbol{A}(\boldsymbol{q})$ is minimized with respect to $\boldsymbol{q}$. Thus the loss of strong ellipticity may be stated as

$$f(\boldsymbol{q}) := \det \boldsymbol{A}(\boldsymbol{q}), \quad \min_{\boldsymbol{q}} f(\boldsymbol{q}) = 0, \quad \boldsymbol{n}(\boldsymbol{q}) \in S^2. \tag{2.17}$$

If the determinant function $f(\boldsymbol{q})$ is differentiable, the minimization problem can be rewritten equivalently as

$$\frac{\partial f}{\partial \boldsymbol{q}}(\boldsymbol{q}) = \boldsymbol{0}, \tag{2.18}$$

which can be solved by standard numerical optimization techniques, *e.g.* a Newton-type iterative procedure.

3 Parametrizations for Bifurcation Analysis

Efficient computation of the minimization problem (2.18) requires a careful choice of the parametrization for the normal vector $\boldsymbol{n}(\boldsymbol{q}) \in S^2$, which is equivalent to select a parametrization for the unit sphere. This choice has a significant effect on the complexity of the determinant function $f(\boldsymbol{q})$ and its derivatives with respect to $\boldsymbol{q}$ needed to solve the optimization problem. Herein, five different options are explored. The first four (spherical, stereographic, projective, tangent) are indeed parametrizations of the unit sphere. The last parametrization, which we term Cartesian, relaxes the restriction that the normal vector be an element of the unit sphere. We describe the parametrizations in detail next, assuming that a Cartesian frame of reference originates from the center of each one.

3.1 Spherical Parametrization

Elements $\boldsymbol{n}$ of the unit sphere S^2 are simply parametrized by their spherical coordinates with polar angle $\varphi \in [0, \pi]$, azimuthal angle $\theta \in [0, \pi]$ and radial distance $r = \|\boldsymbol{n}\| = 1$. The reduced range in the angle θ is due to symmetry of the bifurcation condition, as for this purpose $\boldsymbol{n} = -\boldsymbol{n}$, see Figure 1(a). In terms of the canonical basis

$$\boldsymbol{n}(\varphi, \theta) := \begin{Bmatrix} \sin\varphi \sin\theta \\ \cos\varphi \\ \sin\phi \cos\theta \end{Bmatrix}. \tag{3.1}$$

3.2 Stereographic Parametrization

The unit sphere is parametrized with the aid of an equatorial plane as shown in Figure 1(b). Consider a point P that is both on this plane and on a line that passes through the north pole Q of the sphere and the tip of the vector $\boldsymbol{n}$. The Cartesian coordinates x and y of P provide the desired parametrization, which can be easily derived by finding the intersection of the line and the sphere. The upper hemisphere can be ignored due to the symmetry of the

bifurcation condition, thus avoiding the singularity in parametrizing a normal vector that points to the north pole Q. The normal vector $\boldsymbol{n}$ in terms of the canonical basis is

$$\boldsymbol{n}(x,y) := \left\{ \begin{array}{c} \dfrac{2x}{x^2+y^2+1} \\ \dfrac{2y}{x^2+y^2+1} \\ \dfrac{x^2+y^2-1}{x^2+y^2+1} \end{array} \right\}. \tag{3.2}$$

3.3 Projective Parametrization

In the projective parametrization, the norm of the position vector of a point P with respect to the center of the sphere is constrained to obtain a unit vector $\boldsymbol{n}$ [17]. This is equivalent to project the point P onto the unit sphere S^2, as shown in Figure 1(c). The normalization is effected by means of a constraint enforced by a Lagrange multiplier as

$$\boldsymbol{n}(x,y,z) := \left\{ \begin{array}{c} x \\ y \\ z \end{array} \right\}, \quad \text{subjected to } x^2+y^2+z^2 = 1. \tag{3.3}$$

3.4 Tangent Parametrization

This parametrization of the unit sphere is defined by a tangent plane [19]. Let $\boldsymbol{u} \in \mathbb{R}^3$ be the position vector of the point P in the tangent plane with respect to the contact point Q between the sphere and the plane, then let $\boldsymbol{e} \in S^2$ be the position vector of the contact point Q with respect to the center of the sphere O, as shown in Figure 1(d). Define a rotation vector $\boldsymbol{\theta} := \boldsymbol{e} \times \boldsymbol{u}$, then the rotation angle is $\theta := \|\boldsymbol{\theta}\| \equiv \|\boldsymbol{u}\|$. Let also $\check{\boldsymbol{\theta}} \in so(3)$ be the skew-symmetric tensor such that $\check{\boldsymbol{\theta}} \cdot \boldsymbol{v} \equiv \boldsymbol{\theta} \times \boldsymbol{v} \; \forall \; \boldsymbol{v} \in \mathbb{R}^3$. The expression for the exponential map for $\check{\boldsymbol{\theta}}$ is

$$\exp \check{\boldsymbol{\theta}} := \begin{cases} \boldsymbol{I} \in SO(3), & \text{if } \theta = 0; \\ \boldsymbol{I} + \dfrac{\sin\theta}{\theta}\check{\boldsymbol{\theta}} + \dfrac{(1-\cos\theta)}{\theta^2}\check{\boldsymbol{\theta}}^2 \in SO(3), & \text{if } \theta > 0; \end{cases} \tag{3.4}$$

which is often accredited to Rodrigues [7]. Next define

$$\exp_{\boldsymbol{e}} \boldsymbol{u} := \exp \check{\boldsymbol{\theta}} \cdot \boldsymbol{e} = \cos\theta \boldsymbol{e} + \frac{\sin\theta}{\theta}\boldsymbol{u} \in S^2. \tag{3.5}$$

The parametrization follows immediately by setting the contact point Q to the north pole of the sphere, *i.e.* $\boldsymbol{e} = [0,0,1]^T$ and $\boldsymbol{u} = [x,y,0]^T$ with the normal vector $\boldsymbol{n}$ given by

$$\boldsymbol{n} = \exp_{\boldsymbol{e}} \boldsymbol{u} \in S^2. \tag{3.6}$$

which leads to a more explicit representation for the normal vector in the canonical basis as

$$\boldsymbol{n}(x,y) := \left\{ \begin{array}{c} \dfrac{x \sin\sqrt{x^2+y^2}}{\sqrt{x^2+y^2}} \\ \dfrac{y \sin\sqrt{x^2+y^2}}{\sqrt{x^2+y^2}} \\ \cos\sqrt{x^2+y^2} \end{array} \right\}. \tag{3.7}$$

3.5 Cartesian Parametrization

The strong ellipticity condition

$$(\boldsymbol{u} \otimes \boldsymbol{v}) : \mathbb{C} : (\boldsymbol{u} \otimes \boldsymbol{v}) > 0, \quad \forall\, \boldsymbol{u}, \boldsymbol{v} \in \mathbb{R}^3 \setminus \{\boldsymbol{0}\} \tag{3.8}$$

only requires that the vectors $\boldsymbol{u}$ and $\boldsymbol{v}$ be non-zero. Thus, the condition that they belong to the unit sphere S^2 may be relaxed. In analogy to the classical acoustic tensor (2.14), define

$$\boldsymbol{B} := \boldsymbol{v} \cdot \mathbb{C} \cdot \boldsymbol{v} \quad \text{or} \quad B_{jk} := v_i C_{ijkl} v_l, \quad \boldsymbol{v} \in \mathbb{R}^3 \setminus \{\boldsymbol{0}\}, \tag{3.9}$$

thus the strong ellipticity condition may be expressed as

$$\boldsymbol{u} \cdot \boldsymbol{B} \cdot \boldsymbol{u} > 0, \quad \boldsymbol{u} \in \mathbb{R}^3 \setminus \{\boldsymbol{0}\}. \tag{3.10}$$

As in (2.16), the strong ellipticity condition becomes

$$\det \boldsymbol{B} > 0. \tag{3.11}$$

Proposition 1. *The tensor $\boldsymbol{B}$ from (3.9) leads to the same bifurcation condition than the acoustic tensor $\boldsymbol{A}$ from (2.14).*

Proof. Introduce the bijective map $g : \mathbb{R}^3 \setminus \{\boldsymbol{0}\} \mapsto S^2 \times \mathbb{R}^+$ that allows the representation of nonzero vectors in $\mathbb{R}^3$ as unit vectors in the unit sphere (direction) and the corresponding nonzero norm (magnitude). Then define

$$\boldsymbol{v} \in \mathbb{R}^3 \setminus \{\boldsymbol{0}\}, \quad v := \|\boldsymbol{v}\| \in \mathbb{R}^+, \quad \boldsymbol{n} := \frac{\boldsymbol{v}}{v} \in S^2, \tag{3.12}$$

therefore from (2.15) and (3.10)

$$\boldsymbol{B}(v,\boldsymbol{n}) = v^2 \boldsymbol{A}(\boldsymbol{n}) \quad \text{and} \quad \det \boldsymbol{B}(v,\boldsymbol{n}) = v^6 \det \boldsymbol{A}(\boldsymbol{n}). \tag{3.13}$$

Now let the bifurcation condition for $\boldsymbol{A}$ be

$$\min_{\boldsymbol{n}} \det \boldsymbol{A}(\boldsymbol{n}) = 0, \quad \boldsymbol{a} := \arg\min_{\boldsymbol{n}} \det \boldsymbol{A}(\boldsymbol{n}) \in S^2, \quad \det \boldsymbol{A}(\boldsymbol{n}) > 0 \,\forall\, \boldsymbol{n} \neq \boldsymbol{a}, \tag{3.14}$$

then it follows from (3.13) that

$$\det \boldsymbol{B}(s,\boldsymbol{a}) = 0, \quad \det \boldsymbol{B}(s,\boldsymbol{n}) > 0, \quad \forall\, \boldsymbol{n} \neq \boldsymbol{a} \text{ and } \forall\, s \in \mathbb{R}^+, \tag{3.15}$$

which means that

$$\min_{v,\boldsymbol{n}} \det \boldsymbol{B}(v,\boldsymbol{n}) = 0, \quad \{s,\boldsymbol{a}\} := \arg\min_{v,\boldsymbol{n}} \det \boldsymbol{B}(v,\boldsymbol{n}) \,\forall\, s \in \mathbb{R}^+, \tag{3.16}$$

as required. □

In order to remove the multiple minima associated with the arbitrary value of the scalar parameter s and obtain a parametrization, we restrict the range of the Cartesian coordinates such that $x, y, z \in [-1, 1]$ and set the normal vector to

$$\boldsymbol{v}(x,y,z) := \begin{cases} [x,y,1]^T, & \text{if } x \in [-1,1] \text{ and } y \in [-1,1); \\ [1,y,z]^T, & \text{if } y \in [-1,1] \text{ and } z \in [-1,1); \\ [x,1,z]^T, & \text{if } z \in [-1,1] \text{ and } x \in [-1,1); \\ [1,1,1]^T, & \text{otherwise .} \end{cases} \tag{3.17}$$

This confines the normal vector to the cube of side length 2 centered at the origin as shown in Figure 1(e). Only three faces of the cube need to be considered due to the symmetry of the bifurcation condition.

4 Bifurcation Detection

Within an incremental update setting, the detection of the bifurcation condition for each time increment using any of the parametrizations just described may be effected by the following procedure:

- An initial coarse sampling is performed over the parametric space for $\boldsymbol{q}$ for the normal vector $\boldsymbol{n} \in S^2$ or $\boldsymbol{v} \in \mathbb{R}^3 \setminus \{\boldsymbol{0}\}$ associated with the parametrization. This leads to a coarse estimate of the determinant function $f(\boldsymbol{q})$.
- The coarse estimate is used to initiate a Newton-type iterative procedure to find a better approximation to the minimum.

This simple procedure may not yield estimates of the bifurcation condition that are accurate enough. One way to improve the solution is to introduce adaptive time increments. Define

$$\mu_n := \min_{\boldsymbol{q}} f_n(\boldsymbol{q}) = \min_{\boldsymbol{q}} \det \boldsymbol{B}_n(\boldsymbol{q}) \tag{4.1}$$

where the tensor $\boldsymbol{B}_n(\boldsymbol{q})$ may be either the one from (2.14) or the one from (3.9), depending on the parametrization in use, and the index n indicates that the evaluation occurs at time t_n.

Consider the original time increment from t_n to t_{n+1}, where $\mu_n > 0$ and $\mu_{n+1} < 0$. This means that between time t_n and t_{n+1}, the strong ellipticity condition is violated and hence

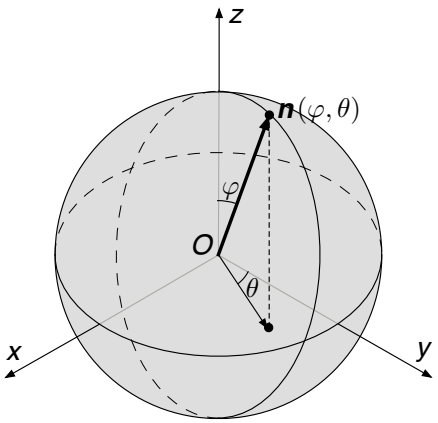

(a) Spherical

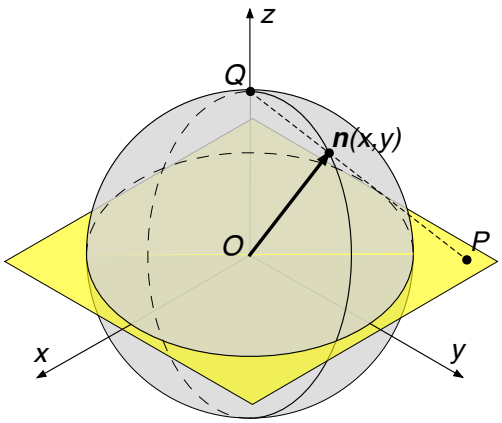

(b) Stereographic

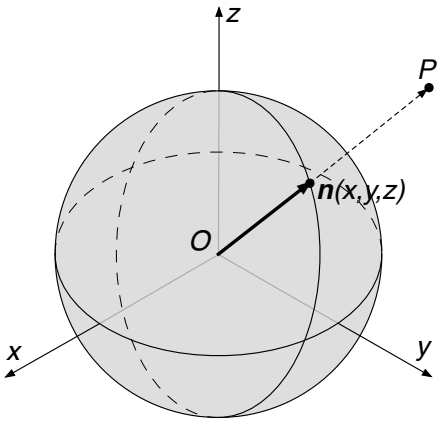

(c) Projective

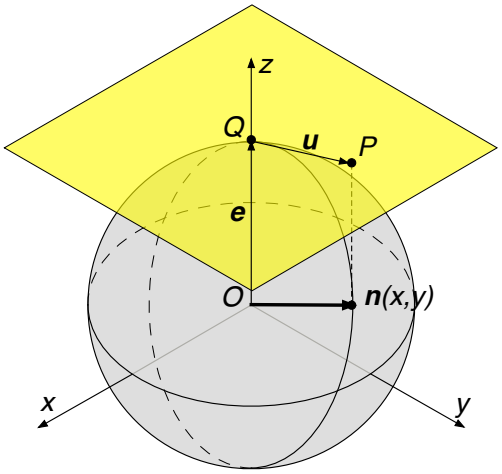

(d) Tangent

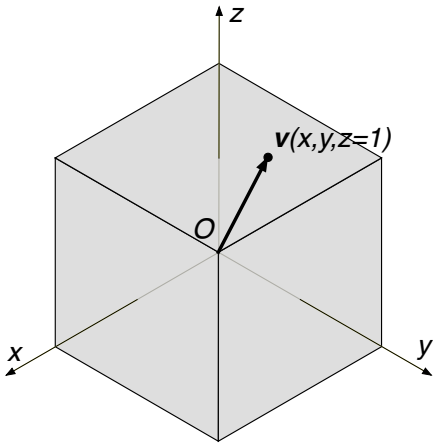

(e) Cartesian

Figure 1: Parametrizations.

material bifurcates. Assume also that $\mu_n/\mu_0 > \epsilon$, where μ_0 is the value of the determinant function evaluated at time t_0 and ϵ is a target tolerance. We wish to find a better estimate for the determinant function μ_n, and hence the bifurcation time t_n, such that $\mu_n/\mu_0 \leq \epsilon$. This is achieved by an adaptive time increment procedure by means of bisection, as shown in Algorithm 1. This algorithm essentially cut the time increment to half until the convergence criteria $\mu_n/\mu_0 \leq \epsilon$ is met.

Algorithm 1 AdaptiveStep$(\mu_0, \mu_{n+1}, t_{n+1}, \epsilon)$

Require: $\mu_{n+1} < 0$
Ensure: $\mu_{n+1,k} \in [0, \epsilon\mu_0]$
  initialize $k \leftarrow 1, \quad \alpha \leftarrow \frac{1}{2}, \quad \triangle t \leftarrow t_{n+1} - t_n, \quad \mu_{n+1,k} \leftarrow \mu_{n+1}$
  while $\mu_{n+1,k} < 0$ **or** $\mu_{n+1,k}/\mu_0 > \epsilon$ **do**
    $t_{n+1,k} \leftarrow t_n + \alpha\triangle t$
    compute $\boldsymbol{F}(t_{n+1,k})$ using the global solution scheme
    compute $\triangle\boldsymbol{Z}(t_{n+1,k})$ by solving (2.11)
    compute $\mathbb{C}(t_{n+1,k})$ using (2.12)
    compute $\mu_{n+1,k}$ by solving (4.1)
    if $\mu_{n+1,k} > 0$ **then**
      $\alpha \leftarrow \alpha + 2^{-k}$
    else
      $\alpha \leftarrow \alpha - 2^{-k}$
    end if
    $k \leftarrow k + 1$
  end while

The adaptive time increment procedure allows the accurate (up to the tolerance ϵ) detection of bifurcation time during a loading process.

5 Numerical Examples

The performance and applicability of the parametrizations described in Section 3 are examined by applying them to the bifurcation analysis of several material models under different loading conditions. The analysis is performed at the material point level. Of particular interest are the robustness and computational efficiency of different parametrizations.

5.1 Small deformation isotropic elastic damage model

We start with the bifurcation analysis on a simple isotropic damage model under infinitesimal deformation. The model formulation is briefly presented in the next section.

5.1.1 Model formulation

The strain-energy function of the isotropic damage model is assumed to have the following form

$$\Psi(\boldsymbol{\epsilon}^e, \xi) = \frac{1}{2}(1-\xi)\boldsymbol{\epsilon}^e : \mathbb{C}^e : \boldsymbol{\epsilon}^e \tag{5.1}$$

where $\boldsymbol{\epsilon}^e$ is the infinitesimal elastic strain tensor, ξ is a damage parameter and $\mathbb{C}^e$ is the fourth-order elastic modulus. For isotropic linear elasticity

$$\mathbb{C}^e = \lambda \boldsymbol{\delta} \otimes \delta + 2\mu \boldsymbol{I} \tag{5.2}$$

where λ and μ are Lamé constant and shear modulus, respectively. $\boldsymbol{\delta}$ is the second-order identity tensor, $(\boldsymbol{I})_{ijkl} = 1/2(\delta_{ik}\delta_{jl} + \delta_{il}\delta_{jk})$ is the fourth-order symmetric identity tensor.

We adopt the following evolution law for the scalar damage parameter ξ [10]

$$\xi(\alpha) = \xi_\infty[1 - \exp(-\alpha/\tau)] \tag{5.3}$$

where ξ_∞ describes the dimensionless maximum damage and τ is referred to as the damage saturation parameter. $s \in [0, t]$ denotes the history variable. The parameter α is the maximum thermodynamic force [10]

$$\alpha(t) = \max_{s\in[0,t]} \Psi_0(s) \tag{5.4}$$

where $\Psi_0(s)$ is the undamaged strain energy at time s.

Given the strain-energy function (5.1) and the damage evolution (5.3), the fourth-order tangent modulus can be derived by taking 2nd derivative of the strain-energy function with respect to strain measure $\boldsymbol{\epsilon}_e$, which results in

$$\mathbb{C} = (1-\xi)\mathbb{C}^e - \beta\frac{\partial \xi}{\partial \alpha}(\boldsymbol{\sigma}_0 \otimes \boldsymbol{\sigma}_0) \tag{5.5}$$

where $\beta \neq 0$ if and only if damage evolves within the time increment.

5.1.2 Simple shear test

TODO: add simple shear test results

5.2 Finite deformation anisotropic hyperelastic damage model

In this section, a finite deformation anisotropic hyperelastic damage model is analyzed for material bifurcation. By adding complexity to the material model, and hence the tangent modulus, we would like to study how is the performance of different parametrizations effected, especially in terms of the computational cost and robustness. The key feature of the model is first proposed.

5.2.1 Model formulation

The free energy function of the finite-deformation anisotropic hyperelastic damage model consists of an isotropic term and direction- dependent terms. This type of energy formulation is motivated to capture behavior of materials with a isotropic matrix and some microfibers with preferred directions, such as the model proposed by [5] to capture behavior of hydrided nuclear cladding materials. We assume that the damage affects both the matrix and the microfibers. The free energy function is proposed to have the following form:

$$\Psi(\boldsymbol{C}, \boldsymbol{M}, \xi_m, \xi_i) = (1 - \xi_m)\Psi_m^0(\boldsymbol{C}) + \sum_i^n (1 - \xi_i)\Psi_i^0(\boldsymbol{C}, \boldsymbol{M}) \tag{5.6}$$

where $\boldsymbol{C}$ is the Right Cauchy-Green tensor, $\boldsymbol{M}$ is a unit vector characterizing the preferred fiber direction. ξ_m and ξ_i are the damage factors corresponding to the matrix and the ith fibers, respectively. In the following examples, we assume that there are two preferred fiber directions, i.e., $n = 2$.

We adopt a compressible Neo-Hookean type energy function for the effective (undamaged) matrix component

$$\Psi_m^0(\boldsymbol{C}) = \frac{1}{8}\lambda(\ln I_3)^2 - \frac{1}{2}\mu \ln I_3 + \frac{1}{2}\mu(I_1 - 3) \tag{5.7}$$

where λ and μ are Lamé's constant and shear modulus, respectively.

For microfibers, we adopt one particular form of strain-energy function ([11])

$$\Psi_i^0(\boldsymbol{C}, \boldsymbol{M}) = \frac{k_i}{q_i}\{\exp[q_i(I_4 - 1)^2]\} \tag{5.8}$$

where k_i and q_i are elastic constants for the ith fiber. The strain invariants I_1, I_3 and I_4 are defined as

$$I_1 = \operatorname{tr} \boldsymbol{C}, \tag{5.9}$$

$$I_3 = \det \boldsymbol{C}, \tag{5.10}$$

$$I_4 = \boldsymbol{M} \cdot (\boldsymbol{C}\boldsymbol{M}) \tag{5.11}$$

For damage evolution, the same evolution law as in (5.3) is used, except that for each phase of the material, i.e., each of the matrix and fibers, there will be a different set of parameters for damage evolution ([5]).

Given the energy function (5.6), the 4th order tangent needed for bifurcation analysis can be derived by taking derivative of the energy function with respect to some strain measures, in particular

$$\tilde{\mathbb{C}} = (1 - \xi_m)\tilde{\mathbb{C}}_m^0 + \sum_i^n (1 - \xi_i)\tilde{\mathbb{C}}_i^0 - \beta_m \xi_m'(\boldsymbol{S}_m^0 \otimes \boldsymbol{S}_m^0) - \sum_i^n \beta_i \xi_i'(\boldsymbol{S}_i^0 \otimes \boldsymbol{S}_i^0) \tag{5.12}$$

where $\beta_m \neq 0$ if and only if damages evolves in matrix, and $\beta_i \neq 0$ if and only if damages evolves in fiber i. The effective tangent modulus tensor is given by

$$\tilde{\mathbb{C}}_m^0 = 4\frac{\partial^2 \Psi_m^0}{\partial \boldsymbol{C} \partial \boldsymbol{C}} \tag{5.13}$$

$$\tilde{\mathbb{C}}_i^0 = 4\frac{\partial^2 \Psi_i^0}{\partial \boldsymbol{C} \partial \boldsymbol{C}} \tag{5.14}$$

It should be noted that the 4th-order tangent $\tilde{\mathbb{C}}$ from (5.12) is computed as the derivative of strain energy with respect to the right Cauchy-Green tensor. The strong ellipticity condition (2.13) requires the tangent $\mathbb{C}$ to be computed as a derivative with respect to the deformation gradient. These two tangents can be converted using the following relation (in indicial notation)

$$\mathbb{C}_{ijkl} = S_{lj}\delta_{ik} + F_{ip}\tilde{\mathbb{C}}_{pjlq}F_{kq} \tag{5.15}$$

where $\boldsymbol{S}$ is the 2nd Piola-Kirchhoff tensor, $\boldsymbol{\delta}$ is the Kronecker delta and $\boldsymbol{F}$ is the deformation gradient.

5.2.2 Uniaxial tension test

The finite deformation anisotropic model is tested under monotonically increased uniaxial tension test. The material properties for both matrix and fibers are listed in Table 1.

Matrix:		*Fibers:*	
Lamé's constant	$\lambda = 80$	Elasticity constants	$k_1 = k_2 = 100$
Shear modulus	$\mu = 80$	Elasticity constants	$q_1 = q_2 = 1.0$
Damage variable	$\xi_{\infty(m)} = 1.0$	Damage variable	$\xi_{\infty(1)} = \xi_{\infty(2)} = 1.0$
Damage variable	$\tau_m = 4.0$	Damage variable	$\tau_1 = \tau_2 = 4.0$
		Direction vector	$\boldsymbol{M}_1 = \{0.8,\ 0.6,\ 0.0\}$
			$\boldsymbol{M}_2 = \{0.8, -0.6,\ 0.0\}$

Table 1: Material properties for anisotropic damage model

6 Concluding remarks on material point simulations

Summarizing results from numerical bifurcationa analyses on all three material models, it is found that:

1. The spherical parametrization is the most efficient in terms of computational cost given the same initial sampling interval, provided that the initial sampling is fine enough and the initial guess is a good approximate to the global minimum;

2. The cube parametrization is the most robust one, for all the material models and sampling intervals, cube parametrization is able to converge and detect bifurcation; it requires very few initial sampling points, which could make up for the computational cost;

3. The Lagrange parametrization has similar computational cost as cube parametrization, but far less robust.

4. The stereographic and exponential parametrization are the least robust parametrizations, i.e., they are more likely to have convergence issues, which is expected given the complicated shape of the minimization function $\det \boldsymbol{A}$.

References

[1] S. Antman. *Nonlinear Problems in Elasticity*. Springer, New York, second edition, 2005.

[2] F. Armero and K. Garikipati. An analysis of strong discontinuities in multiplicative finite strain plasticity and their relation with the numerical simulation of strain localization in solids. *International Journal of Solids and Structures*, 33(20-22):2863–2885, Aug 1996. ISSN 0020-7683. doi: {10.1016/0020-7683(95)00257-X}.

[3] R. Becker. Ring fragmentation predictions using the Gurson model with material stability conditions as failure criteria. *International Journal of Solids and Structures*, 39(13-14):3555–3580, Jun-Jul 2002. ISSN 0020-7683. doi: {10.1016/S0020-7683(02)00170-1}. Symposium on Material Instabilities and the Effect of Microstructure, UNIV TEXAS, AUSTIN, AUSTIN, TEXAS, MAY 07-11, 2001.

[4] N. Bleier and J. Mosler. Efficient variational constitutive updates by means of a novel parameterization of the flow rule. *International Journal for Numerical Methods in Engineering*, 89(9):1120–1143, Mar 2 2012. ISSN 0029-5981. doi: {10.1002/nme.3280}.

[5] Qiushi Chen, Jakob T Ostien, and Glen Hansen. Development of a used fuel cladding damage model incorporating circumferential and radial hydride responses. *Journal of Nuclear Materials*, 447(1):292–303, 2014.

[6] E. Fancello, J.P. Ponthot, and L. Stainier. A variational formulation of constitutive models and updates in non-linear finite viscoelasticity. *International Journal for Numerical Methods in Engineering*, 65(11):1831–1864, Mar 12 2006. ISSN 0029-5981. doi: {10.1002/nme.1525}.

[7] J. Gallier. *Geometric Methods and Applications: For Computer Science and Engineering*. Springer, June 2011. ISBN 9781441999603.

[8] J. Hadamard. *Leçons Sur La Propagation Des Ondes Et Les Équations De L'hydrodynamique*. Hermann, Paris, 1903.

[9] R. Hill. Acceleration Waves in Solids. *Journal of the Mechanics and Physics of Solids*, 10(1):1–16, 1962. ISSN 0022-5096. doi: {10.1016/0022-5096(62)90024-8}.

[10] Gerhard A Holzapfel. *Nonlinear solid mechanics*, volume 24. Wiley Chichester, 2000.

[11] Gerhard A Holzapfel and Ray W Ogden. Constitutive modelling of arteries. In *Proceedings of the Royal Society of London A: Mathematical, Physical and Engineering Sciences*, volume 466, pages 1551–1597. The Royal Society, 2010.

[12] M. Lambrecht, C. Miehe, and J. Dettmar. Energy relaxation of non-convex incremental stress potentials in a strain-softening elastic-plastic bar. *International Journal of Solids and Structures*, 40(6):1369–1391, Mar 2003. ISSN 0020-7683. doi: {10.1016/S0020-7683(02)00658-3}.

[13] C. Miehe, J. Schotte, and M. Lambrecht. Homogenization of inelastic solid materials at finite strains based on incremental minimization principles. Application to the texture analysis of polycrystals. *Journal of the Mechanics and Physics of Solids*, 50(10):2123–2167, Oct 2002. ISSN 0022-5096. doi: {10.1016/S0022-5096(02)00016-9}.

[14] C. Miehe, M. Lambrecht, and E. Gürses. Analysis of material instabilities in inelastic solids by incremental energy minimization and relaxation methods: evolving deformation microstructures in finite plasticity. *Journal of the Mechanics and Physics of Solids*, 52(12):2725–2769, Dec 2004. ISSN 0022-5096. doi: {10.1016/j.jmps.2004.05.011}.

[15] J. Mosler and O.T. Bruhns. On the implementation of rate-independent standard dissipative solids at finite strain - Variational constitutive updates. *Computer Methods in Applied Mechanics and Engineering*, 199(9-12):417–429, 2010. ISSN 0045-7825. doi: {10.1016/j.cma.2009.07.006}.

[16] M. Ortiz and L. Stainier. The variational formulation of viscoplastic constitutive updates. *Computer Methods in Applied Mechanics and Engineering*, 171(3-4):419–444, 1999.

[17] M. Ortiz, Y. Leroy, and A. Needleman. A Finite-Element Method for Localized Failure Analysis. *Computer Methods in Applied Mechanics and Engineering*, 61(2):189–214, Mar 1987. ISSN 0045-7825. doi: {10.1016/0045-7825(87)90004-1}.

[18] J.R. Rice. The Localization of Plastic Deformation. In Koiter, W.T., editor, *Proceedings of the 14th International Congress on Theoretical and Applied Mechanics*, volume 1, pages 207–220, Amsterdam, 1976. North-Holland.

[19] J.C. Simo and D.D. Fox. On a Stress Resultant Geometrically Exact Shell-Model .1. Formulation and Optimal Parametrization. *Computer Methods in Applied Mechanics and Engineering*, 72(3):267–304, MAR 1989. ISSN 0045-7825. doi: {10.1016/0045-7825(89)90002-9}.

[20] T.Y. Thomas. *Plastic Flow and Fracture in Solids*. Academic Press, London, 1961.

[21] C. Truesdell and W. Noll. *The Non-Linear Field Theories of Mechanics*. Springer-Verlag, 3rd edition, 2004. ISBN 0387550984.

[22] K. Weinberg, A. Mota, and M. Ortiz. A variational constitutive model for porous metal plasticity. *Computational Mechanics*, 37:142–152, 2006.